Quantum manipulation of valleys in bilayer graphene

G. Y. Wu,[1,2,*] N.-Y. Lue,[2] and Y.-C. Chen[1]

[1]*Department of Physics, National Tsing-Hua University, Hsin-Chu, Taiwan 30013, Republic of China*

[2]*Department of Electrical Engineering, National Tsing-Hua University, Hsin-Chu, Taiwan 30013, Republic of China*

(Received 5 February 2013; revised manuscript received 19 April 2013; published 18 September 2013)

The valley pseudospin is an inherent electron degree of freedom in graphene. This work establishes a theory for manipulation of valley pseudospins at the quantum level, in bilayer graphene. Two key mechanisms of valley manipulation are proposed and valley-based quantum devices—qubits and field-effect transistors—are implemented based on the mechanisms. This work provides a crucial step in paving the way for the experimental realization (expansion) of valley-based quantum (classical) information processing.

DOI: 10.1103/PhysRevB.88.125422 PACS number(s): 73.22.Pr, 03.67.−a, 72.80.Vp, 85.35.−p

I. INTRODUCTION

Graphene is an atomically thin system of carbon atoms with rich physics. Soon after its discovery,[1] it was realized that electrons in graphene behave as two-dimensional (2D) Dirac fermions, leading to an unusual quantum Hall effect, Klein tunneling, and confinement, as well as an immense potential for various applications,[1–6] including important ones associated with the valley pseudospin graphene brings to the field of electronics.[7] As a novel type of information carrier, this valley degree of freedom has opened up a new realm of electronics—valleytronics—in addition to the charge- or spin-based ones and has added great flexibility to advanced electronic device design, especially in the area of information processing.[7–15]

The valley pseudospin is an inherent property of graphene or, more universally, of a 2D honeycomb crystal. It arises because low-lying carrier states in graphene belong to the two degenerate and independent energy valleys located at inequivalent vertices (K and K') of the hexagonal Brillouin zone, which go into each other under time-reversal-symmetry transformation.[6] This pseudospin is similar to the true physical spin of a spin-$\frac{1}{2}$ particle and in principle should be manipulable at the quantum level (i.e., on an individual carrier basis), leading, for example, to valley-based quantum computing/communications, as well as the expansion of classical information processing. Although this conjecture has been around for some time, its implementation in an experimentally accessible system has yet to be realized.

Generally, for quantum manipulation of electrons, it is often desirable to localize electrons and then apply external fields on them for the manipulation. From this point of view, the gapped system of monolayer graphene grown on hexagonal boron nitride (h-BN) (Ref. 16) has been considered as an example material in the previous works of valley manipulation,[13,14] due to the possibility of opening a gap in the system and providing a gap-caused quantum confinement of carriers with electrical gates as is typically done in the field of semiconductor nanodevices. These works have indeed demonstrated the theoretical feasibility of quantum valley manipulation in gapped graphene. In contrast, the actual growth of gapped graphene/h-BN has yet to overcome the issue in association with the small nevertheless nonvanishing lattice mismatch (∼1.8%) between graphene and h-BN. Due to this mismatch, a superstructure called the moiré pattern appears in practical BN-grown graphene,[17] which displays alternating signs of an energy gap and a percolating zero energy mode, hence rendering graphene/h-BN a gapless structure. In order to open a finite gap in this system, certain nontrivial measures, e.g., a biaxial strain, would have to be taken in order to match the lattices and avoid the formation of a moiré pattern.

Our work here addresses the issue of realizing quantum valley manipulation in an alternative graphene system, with the outline given below.

(a) An experimentally accessible material, bilayer graphene (BLG),[4] is utilized as the system.

(b) A theoretical framework, the effective Schrödinger model, is developed and two key mechanisms for individual valley manipulation are established.

(c) For applications, valley quantum devices, i.e., qubits and field-effect transistors (FETs) in BLG, are demonstrated.

Bilayer graphene becomes gapped under a dc bias, which produces a chemical potential difference between the two layers[4–6] and therefore can be utilized just like semiconductors to make a confined structure, as experimentally demonstrated recently with electrical gate technology.[18,19] This makes it well suited to the purpose of localizing electrons for quantum control such as the application envisioned here.[20] More importantly, BLG as a hexagonal crystal shares with monolayer graphene a crucial property required for valleytronics, e.g., the presence of a valley degree of freedom. However, major differences exist between the two systems in the aspect of valley-dependent physics. In the monolayer case, the physics is underlain by the intralayer C-C hopping whereas that in BLG is dominated by both the intra- and interlayer couplings. This enriches, in the case of bilayer graphene, the valley-dependent physics by providing two valuable parallel mechanisms for valley manipulation—band structure warping and generalized valley-orbit interaction (GVOI)—as derived and respectively demonstrated with qubits and FETs below.

The presentation is organized as follows. In Sec. II we describe the effective Schrödinger theory. In Sec. III we present the structure of a valley-based qubit and discuss how to electrically manipulate it. In Sec. IV we present the structure of a valley FET and its principle of operation. In Sec. V we briefly discuss the issue of valley coherence. In Sec. VI we summarize this work. In the Appendix we provide a brief derivation of the Schrödinger model.

II. EFFECTIVE SCHRÖDINGER THEORY

The theory is based on the one-band Schrödinger model of AB-stacked BLG explained below. We denote the four C atoms in a unit cell as A_1, B_1 (in the first layer) and A_2, B_2 (in the second layer), with B_2 sitting right on the top of A_1. A tight-binding model of AB-stacked BLG is characterized by the parameters Δ, t, γ_1, and γ_3, where 2Δ is the dc bias between the layers and t, γ_1, and γ_3 are, respectively, the hopping between A_1 and B_1 (or A_2 and B_2), A_1 and B_2, and B_1 and A_2. The band structure[4–6] is summarized below and shown in Fig. 1. It consists of four bands and displays electron-hole symmetry. An energy gap 2Δ is opened in the middle. Away from the gap, two distant bands are located at $\pm(\Delta^2+\gamma_1^2)^{1/2}$.

In the limit where $\Delta \ll \gamma_1$, as assumed throughout this work, the full tight-binding model can be reduced, by the Schrieffer-Wolff-type transformation, to a two-band model[4] ($\hbar = 1$)

$$\sum_{j=1,2} H_{ij}(k_x,k_y)\varphi_j = E\varphi_i, \quad i = 1,2,$$

which describes only the conduction and valence bands right around the gap. Here the H_{ij} denote Hamiltonian matrix elements and (k_x, k_y) is the electron wave vector relative to the K/K' point. See the Appendix for the explicit expressions of H_{ij}.

The preceding equation in the two-band model describes a gapped symmetric band dispersion. This is closely analogous to a massive Dirac equation in two dimensions with 2Δ being the mass gap. By this analogy, it can further be reduced, in the nonrelativistic limit where the electron energy $|E| \sim \Delta$, to a Schrödinger-type equation. For $E \sim \Delta$ (i.e., low-lying electrons), this reduction gives

$$(E-\Delta)\varphi \approx [H_0(\tau)+H_1(\tau)]\varphi,$$
$$H_0(\tau) = -\frac{2\Delta}{\gamma_1^2}v_f^2k^2 + \frac{1}{2\Delta}\left(\frac{1}{\gamma_1^2}v_F^4k^4 + v'^2k^2\right) + H_0^{(\text{warping})}(\tau) + V,$$

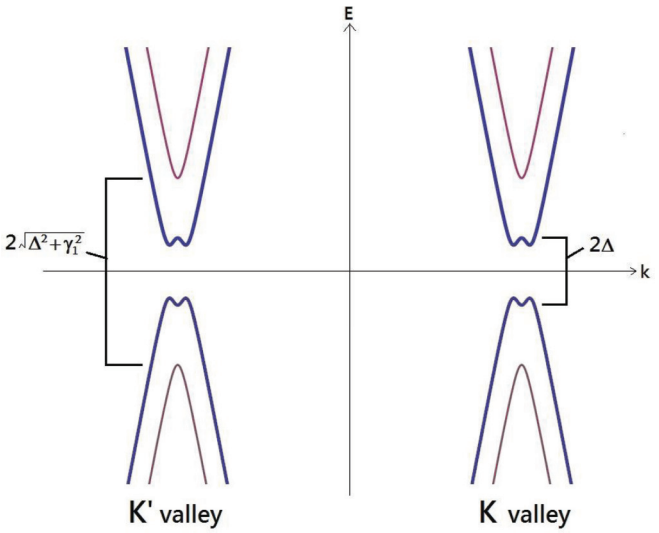

FIG. 1. (Color online) Schematic band structure of bilayer graphene under a dc bias, showing the sombrero structure in the bands and the relative positions of the four bands.

$$H_1(\tau) = H_1^{(\text{warping})}(\tau) + H_1^{(\text{GVOI})}(\tau) + H_1',$$
$$H_0^{(\text{warping})}(\tau) = \tau\frac{v'v_F^2}{\Delta\gamma_1}\left(3k_x^2k_y - k_y^3\right),$$
$$H_1^{(\text{warping})}(\tau) = \tau\frac{v'v_F^2}{\Delta\gamma_1}\left[\frac{2v_F^2}{\gamma_1^2}k^2 - \frac{1}{2\Delta^2}\left(\frac{1}{\gamma_1^2}v_F^4k^4 + v'^2k^2\right)\right] \times \left(3k_x^2k_y - k_y^3\right),$$
$$H_1^{(\text{GVOI})} = \frac{1}{4\Delta^2}\Omega_\tau\{H_{21}[V,H_{12}]_-\},$$
$$H_{12} \equiv \frac{1}{\gamma_1}v_F^2k_+^2 + iv'k_-. \quad (1)$$

Here we have included the presence of a weak slowly varying external electric potential V and made the effective mass approximation with $(k_x, k_y) \to (-i\partial_x, -i\partial_y)$. The above derivation has taken the various relativistic effect ratios, e.g., $|V/\Delta|$ and $|(E-\Delta)/\Delta|$, to be much less than unity and retained only the leading- and next-to-leading-order terms in the equation. The armchair direction is taken to be aligned along the x axis, with $v_F = 3ta/2$ (where v_F is the Fermi velocity and a is the intralayer C-C distance), $v' = 3\gamma_3 a/2$, and $k_\pm \equiv k_x \pm i\tau k_y$ (where τ is the valley index and $+$ and $-$ denote K and K', respectively). We set $t = 2.8$ eV, $\gamma_1 = 0.4$ eV, and $\gamma_3 = 0.3$ eV. Here Ω_τ denotes an operation acting upon the expression following it, by retaining only the τ-dependent terms in the expression.

Equation (1) gives the Schrödinger Hamiltonian H_0 and the first-order relativistic effect H_1. Further, H_1' (not explicitly given above) is the first-order relativistic effect, which is τ independent and irrelevant to the present work. Above $H_0^{(\text{warping})}$ and $H_1^{(\text{warping})}$ produce band warping.[4] In addition, $H_1^{(\text{GVOI})}$ is the GVOI, which reduces, for $v_F = 0$, to $\tau\frac{v'^2}{4\Delta^2}\nabla V \times k$, the simple form of VOI (Refs. 13,14, and 21) in monolayer graphene, which is analogous to the spin-orbit interaction. Note that $H_0^{(\text{warping})}$ and $H_1^{(\text{GVOI})}$ are both τ dependent and as such constitute key mechanisms for valley manipulation. Being valley conserving, they are well suited to valley coherence-sensitive applications.

III. TWO-VALLEY QUBITS

Figure 2 shows a valley-based two-electron qubit, which consists of a pair of laterally coupled quantum dots (QDs) of comparable sizes lying along the x axis in AB-stacked BLG, in the (1, 1) charge configuration. Here V_Δ, V_L, V_R, and V_C are electrical gates, which may be arranged in a mirror-symmetric fashion as suggested here (only those above the graphene layers are explicitly shown). dc biases applied to these gates open energy gaps in the bilayer system and define the QDs.

The logical 0/1 states are represented by the two-valley singlet/triplet S/T_0 states

$$|S\rangle = \frac{1}{\sqrt{2}}(|K_LK_R'\rangle - |K_L'\ K_R\rangle),$$
$$|T_0\rangle = \frac{1}{\sqrt{2}}(|K_LK_R'\rangle + |K_L'\ K_R\rangle),$$
$$|K_LK_R'\rangle \equiv c_{KL}^+c_{K'R}^+|\mathcal{V}\rangle, \quad |K_L'K_R\rangle \equiv c_{K'L}^+c_{KR}^+|\mathcal{V}\rangle.$$

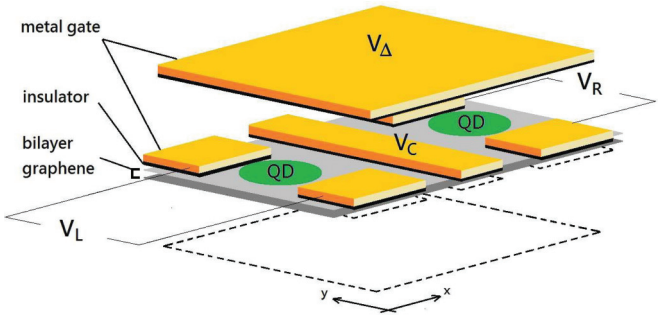

FIG. 2. (Color online) Valley pair qubit consisting of laterally coupled QDs of comparable sizes lying along the x axis in AB-stacked BLG. Here V_Δ, V_L, V_R, and V_C are electrical gates, which may be arranged in a mirror-symmetric fashion as suggested here (only those above the graphene layers are explicitly shown). dc biases applied to these gates open energy gaps in the bilayer system and define the QDs. ac biases applied to V_L/V_R generate R_x. The V_C controls the interdot tunneling t (or the exchange coupling J) and hence R_z.

Here c^+ is the electron creation operator, V denotes vacuum, and K_L (K'_L) and K_R (K'_R) denote the ground states of the K (K') valleys in the left and right QDs, respectively. The electron spins here are taken to be frozen in a triplet state by initialization, as explained below. The initialization starts with the one-QD two-electron state, e.g., $|\mathcal{S}_{1\mathrm{QD}}\rangle \otimes |\mathcal{T}_{\mathrm{spin}}\rangle$ (where $|\mathcal{S}_{1\mathrm{QD}}\rangle$ denotes the one-QD valley singlet and $\mathcal{T}_{\mathrm{spin}}$ the spin triplet) where $|\mathcal{S}_{1\mathrm{QD}}\rangle \equiv |K_R K'_R\rangle$ for example.[22] Then one can adjust the bias of the two QDs such that one of the electrons tunnels into the other QD, transforming the state into the two-QD $|S\rangle \otimes |\mathcal{T}_{\mathrm{spin}}\rangle$. Furthermore, because the spin-orbit interaction in graphene is extremely weak,[6] the spins in the qubit remain coherent for a long time and can be taken to be approximately frozen in the triplet state during qubit manipulation. We thus drop the spin degree of freedom throughout the following discussion. The logical state space of the qubit is isomorphic to the Hilbert space of a spin-$\frac{1}{2}$ system, with the correspondence

$$|S\rangle \Leftrightarrow |\downarrow\rangle, \quad |T_0\rangle \Leftrightarrow |\uparrow\rangle,$$
$$|K_L K'_R\rangle \Leftrightarrow |\rightarrow\rangle, \quad |K'_L K_R\rangle \Leftrightarrow |\leftarrow\rangle,$$

where $\uparrow$, $\downarrow$, $\rightarrow$, and $\leftarrow$ denote up, down, left, and right spin states quantized along the z and x axes of the spin system, respectively. The qubit/spin isomorphism provides a convenient framework to envision the qubit state transformation in terms of an effective spin rotation.

A. Warping-based two-valley manipulation

An arbitrary qubit (or effective spin) rotation can be decomposed into two independent rotations, such as those around the x and z axes. We denote them as $R_x(\theta_x)$ and $R_z(\theta_z)$, respectively, where θ_x and θ_z are the angles of rotation. The corresponding qubit state transformations are given by

$$|K_L K'_R\rangle \to e^{i\theta_x/2}|K_L K'_R\rangle, \quad |K'_L K_R\rangle \to e^{-i\theta_x/2}|K'_L K_R\rangle \tag{2}$$

for $R_x(\theta_x)$ and

$$|T_0\rangle \to e^{i\theta_z/2}|T_0\rangle, \quad |S\rangle \to e^{-i\theta_z/2}|S\rangle \tag{3}$$

for $R_z(\theta_z)$.

First, we discuss the generation of $R_x(\theta_x)$. As Eq. (2) suggests, this may be enabled by introducing a valley-contrasting state evolution in the left QD (or both of the QDs),

$$|K_L\rangle \to e^{i\theta_x/2}|K_L\rangle, \quad |K'_L\rangle \to e^{-i\theta_x/2}|K'_L\rangle. \tag{2'}$$

The valley-contrasting phase θ_x in Eq. (2′) generally vanishes because $|K_L\rangle$ and $|K'_L\rangle$ usually evolve with the same phase due to the valley degeneracy. For a finite θ_x, the symmetry between $|K_L\rangle$ and $|K'_L\rangle$ must be broken. The condition of breaking is discussed below.

1. Warping-based valley symmetry breaking

Valley symmetry breaking can be achieved by applying through V_L (or V_R) to the QD an ac electric field $\varepsilon_{\mathrm{ac}}\sin w_s t$ in the y direction as follows. We ignore the relativistic effect and write the wave equation for the QD state ψ,

$$H_0(t;\tau)\psi(x,y,t;\tau) = i\partial_t\psi(x,y,t;\tau),$$
$$V = V_{\mathrm{QD}} + e\varepsilon_{\mathrm{ac}} y \sin w_s t. \tag{4}$$

Here V_{QD} is the QD confinement potential and the time dependence of H_0 derives from the ac field. The introduction of an ac field breaks time-reversal symmetry. However, the presence of $H_0^{(\mathrm{warping})}$ in H_0 is indispensable for the condition of breaking. Without the term, H_0 would be τ independent and the states of $\tau = \pm$, e.g., $|K_L\rangle$ and $|K'_L\rangle$, would evolve in a τ-independent fashion, giving a vanishing θ_x.

2. Valley-contrasting geometric phase

We apply Eq. (4) to the QD ground state. For $\varepsilon_{\mathrm{ac}} = 0$, the ground-state solution of Eq. (4) is denoted by $\psi_0(x, y, t; \tau)$, with w_0 the energy relative to the conduction band edge. Note that $\psi_0(x, y, t; +) = |K_L\rangle$, $\psi_0(x, y, t; -) = |K'_L\rangle$, and w_0 is τ independent due to time-reversal symmetry. For $\varepsilon_{\mathrm{ac}} \neq 0$, we consider the simple case where $V_{\mathrm{QD}} = \frac{1}{2}mw_0^2(x^2 + y^2)$ (m is a mass parameter) and the ac field is weak and quasistatic with $w_s \ll w_0$. To the leading order in $\varepsilon_{\mathrm{ac}}$, we write the total potential $V \approx V_{\mathrm{QD}}[x, y + y_0(t)]$, which describes a dynamical QD with $-y_0(t) \equiv -e\varepsilon_{\mathrm{ac}} \sin w_s t/mw_0^2$ the dynamical equilibrium position. This admits the simple adiabatic solution[23]

$$\psi(x,y,t;\tau) \approx \psi_0[x,y + y_0(t),t;\tau] \times \exp\left(-i\int_{\mathrm{GP}}^{t}\gamma_0(\tau)dt'\right),$$
$$\psi_0[x,y + y_0(t),t;\tau] = \phi_0[x,y + y_0(t);\tau] \times \exp\left(-i\int_{\mathrm{DP}}^{t} w_0 dt'\right), \tag{5}$$
$$\gamma_0(\tau) \approx \partial_t y_0(t)\langle\varphi_0(x,y;\tau)|k_y\varphi_0(x,y;\tau)\rangle.$$

where GP denotes the geometric phase and DP the dynamical phase.

An intuitive interpretation follows. It is the instantaneous ground state ψ_0 (with the spatial part φ_0 and the temporal part equal to the dynamical phase) observed at the moving QD and transformed back to the laboratory reference frame. The transformation produces an energy shift $\langle\partial_t y_0 k_y\rangle$ (denoted γ_0), which generates the geometric phase. This phase (or γ_0)

is τ dependent, as will be shown in the following section, and therefore is identified with $\theta_x/2$ in Eq. (2′) or (2).

3. *Qubit rotation rate*

Since γ_0 generates the geometric phase, the typical qubit rotation rate is given by γ_0. We derive γ_0 with perturbation theory, treating the warping term in H_0 as a perturbation. To leading order this yields[24]

$$\gamma_0(\tau) \approx [2\partial_t y_0(t)] \times \sum_n \frac{\langle 0|H_0^{(\text{warping})}(\tau)|2n+1\rangle\langle 2n+1|k_y|0\rangle}{w_0^{(0)} - w_{2n+1}^{(0)}},$$
$$H_0^{(0)}|n\rangle = w_n^{(0)}|n\rangle, \tag{6}$$
$$H_0^{(0)} \equiv -\frac{2\Delta}{\gamma_1^2}v_f^2k^2 + \frac{1}{2\Delta}\left(\frac{1}{\gamma_1^2}v_F^4k^4 + v'^2k^2\right) + V_{\text{QD}}.$$

Here $H_0^{(0)}$ is the QD Hamiltonian H_0 with the warping term removed. The above expression shows an explicit τ dependence on γ_0 that derives from the warping term. For an order-of-magnitude estimate, we set the QD size $L \sim 300$ Å, $\Delta \sim 5$ meV, $\pi/w_s \sim 0.1$ ns, $\hbar w_0 \sim m w_0^2 L^2 \sim O$ (meV), and $e\varepsilon_{\text{ac}}/m w_0^2 \sim 0.3$ L. This yields $\gamma_0 \sim 1$ GHz, leading to the prospect of operating valley qubits in the GHz range.

The two-valley qubit is analogous to a two-spin qubit[25] and hence shares[13] the advantages of the latter in several aspects, summarized below. First, it has a decoherence-free logical state space. This means that the qubit is noise resistant to long-wavelength or low-frequency electric potential fluctuations.[26] Second, R_z can be generated by utilizing the exchange coupling (denoted J) between the two localized electrons in the qubit. With $J \sim 4t^2/U$ (where t denotes interdot tunneling and U on-site Coulomb repulsion), this gives a way to control R_z, e.g., by tuning the interdot tunneling. Finally, two valley qubits can be placed side by side to form a CPHASE gate; R_x, R_z, and the CPHASE gate constitute universal quantum computing.[27–29]

IV. VALLEY FETS

Figure 3(a) shows a valley FET in gapped AB-stacked BLG. The source and drain are armchair graphene nanoribbons (AGNRs) and the channel is a graphene quantum wire (QW) aligned in the armchair direction and subject to the control of a side gate bias. The bias produces in the channel an in-plane electric field in the y direction.

In both the leads, the unique boundary condition in an AGNR mixes K and K' valleys in a 50-50 ratio, giving the lead subband state as symbolically represented by $(|K\rangle + S|K'\rangle)/2^{1/2}$,[30] where $S = \pm 1$ is subband dependent. This determines the specific valley polarization injected into the channel and detected at the drain.

A. The GVOI-based valley precession

The GVOI in the channel provides a key mechanism to switch on/off the FET with the gate bias as follows. Under the bias, the energy subbands in the channel are valley split due to the GVOI (as shown below), giving a wave-vector difference $k_+ - k_-$ between the states of $\tau = \pm$, as shown in Fig. 3(b). Therefore, after a source electron is injected into the channel, the two valley components in the electron evolve with different phases, leading to the channel state $(e^{i\varphi(x)}|K\rangle + S|K'\rangle)/2^{1/2}$. The phase difference $\varphi(x) = (k_+ - k_-)x$ here increases linearly with the distance x traveled. This describes an electron precession in the valley space, with φ the precession angle. At the end of the channel ($x = L$), depending on $\varphi = 2n\pi$ [$(2n+1)\pi$], the channel and drain polarizations are parallel [orthogonal], admitting [blocking] the electron into [off] the drain. The GVOI here plays a role similar to the spin-orbit interaction (SOI) utilized in a spin FET,[31] to achieve the on-off switch function.

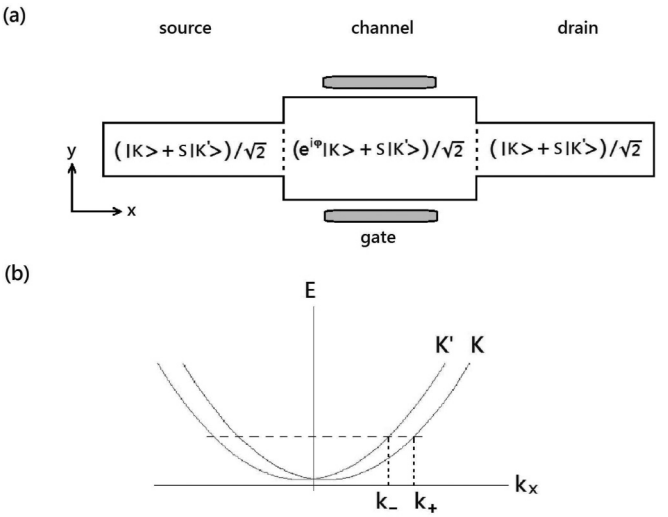

FIG. 3. (a) Schematic plot of the valley FET in AB-stacked BLG, with AGNR source and drain and a graphene QW channel (aligned in the armchair direction) subject to the control of a side gate bias. In order to define the QW, the side gates and/or vertical gates (such as V_Δ in Fig. 2, but not shown here) can be arranged in a mirror-symmetric fashion, as in Fig. 2, with dc biases applied upon them. Electron states in the various regions are also shown. (b) Under the gate bias, energy subbands in the channel are valley split due to the GVOI, giving a wave-vector difference $k_+ - k_-$ between the states of $\tau = \pm$.

We derive the GVOI-based valley splitting/precession in the channel. In the present case, we write $H_1^{(\text{GVOI})}$ in Eq. (1) explicitly, with

$$H_1^{(\text{GVOI})} = i\tau\frac{v'^2}{4\Delta^2}k_x\underline{k_yV} - i\tau\frac{v_F^4}{2\Delta^2\gamma_1^2}k_x\left(\underline{k_y^2Vk_y} + \underline{k_yVk^2}\right) + \tau\frac{v'v_F^2}{4\Delta^2\gamma_1}\left(\underline{k_y^3V} + \underline{2k_y^2Vk_y}\right).$$

The underlined expressions in $H_1^{(\text{GVOI})}$ are evaluated first. Here k_x is the electron wave vector along the channel and the potential V is y dependent only, e.g., $V = V_{\text{QW}}(y) + e\varepsilon_y y$, with $V_{\text{QW}}(y) = \frac{1}{2}mw_0^2y^2 - Dy^4$ being the QW confinement potential. Here ε_y is the gate field applied, w_0 is the subband edge, and the quartic term $-Dy^4$ is introduced such that V_{QW} simulates a realistic, finite confinement potential that flattens out at distant y. Without the quartic term, the gate field would only shift V_{QW} to a new equilibrium position without producing any effect.

The valley degeneracy is lifted by ε_y due to the GVOI. This can be deduced by a symmetry argument based on $H_1^{(\mathrm{GVOI})}$: The odd-in-k_x τ-dependent terms in $H_1^{(\mathrm{GVOI})}$ remove the valley degeneracy at a given k_x. For a quantitative estimate of the splitting, we take $H_0^{(0)}$ and $|n\rangle$ in the qubit discussion (with the replacement $V_{\mathrm{QD}} \to \frac{1}{2}mw_0^2y^2$ for the QW confinement) as the unperturbed Hamiltonian and eigenstates, respectively, and $e\varepsilon_y y$, Dy^4, and $H_1^{(\mathrm{GVOI})}$ as perturbations.[32] This yields (with m^* the subband effective mass)

$$k_+ - k_- = -\frac{2m^*\alpha_{\mathrm{vo}}}{\hbar^2}, \quad \varphi = -\frac{2m^*\alpha_{\mathrm{vo}}}{\hbar^2}L,$$

$$\begin{aligned}\alpha_{\mathrm{vo}}/\varepsilon_y \approx{}& \frac{-ev_F^4 D}{\Delta^2\gamma_1^2}\sum_n{\sum}'\langle 0|k_y^2|2n\rangle \\ &\times \langle 2n|y^4|0\rangle \big/ \left(w_0^{(0)} - w_{2n}^{(0)}\right) \\ &+ \frac{2eD}{\Delta^2}\sum_n \langle 0|\left[\frac{2v_F^4}{\gamma_1^2}\left(3iy^2k_y + y^3k_y^2\right) + v'^2y^3\right] \\ &\times |2n+1\rangle\langle 2n+1|y|0\rangle \big/ \left(w_0^{(0)} - w_{2n+1}^{(0)}\right), \qquad (7)\end{aligned}$$

where α_{vo} is the Rashba constant due to the GVOI. As shown above, α_{vo} is ε_y dependent, which permits the electric control of valley precession angle. We estimate α_{vo} using the following parameters: the QW width $W \sim 300$ Å, $\Delta \sim 5$ meV, and $\hbar w_0 \sim mw_0^2W^2 \sim e\varepsilon_y \mathrm{W} \sim DW^4 \sim O$ (meV). This yields α_{vo} in the range 10^{-12}–10^{-11} eV m, comparable to the large SOI-caused Rashba constant in InAs.[33] By analogy to spin FETs, valley FETs thus carry similar potential advantages in building low-power high-density integrated circuits.

V. VALLEY COHERENCE

Finally, we briefly note the issue of valley coherence here. As it is primarily limited by the intervalley $K \leftrightarrow K'$ scattering, an in-plane process in nature,[34] we estimate the valley coherence time in AB-stacked BLG with that in monolayer graphene,[13] due to similar in-plane properties in the two cases. This gives, in a typical application, the coherence time in the range of μs or longer, which is sufficiently long for valley manipulation in AB-stacked BLG and makes it possible to quantum control individual valleys for the realization (expansion) of valley-based quantum (classical) information processing.

VI. SUMMARY

We have established the theory for manipulation of valley pseudospins at the quantum level, in bilayer graphene. We have proposed two key mechanisms of valley manipulation, which are based on the band-structure warping and the generalized valley-orbit interaction, respectively. Quantum valleytronic devices—qubits and FETs—are implemented utilizing these mechanisms. This work provides a crucial step in paving the way for the experimental realization (expansion) of valley-based quantum (classical) information processing.

ACKNOWLEDGMENT

We would like to thank the ROC National Science Council for support through Contract No. NSC101-2112-M-007-012.

APPENDIX: DERIVATION OF THE SCHRÖDINGER MODEL FOR BILAYER GRAPHENE

In this Appendix we derive the Schrödinger model, as expressed in Eq. (1). We start with the two-band model for the conduction band and the valence band around the band gap, which has been derived in Ref. 4. We extend the model to include the effect of an external slowly varying field $V(x,y)$, which modulates the band edges and leads to the Hamiltonian

$$H = \begin{pmatrix} -\Delta + V + \frac{2\Delta}{\gamma_1^2}v_f^2|k|^2 & \frac{1}{\gamma_1}v_F^2k_+^2 + iv'k_- \\ \frac{1}{\gamma_1}v_F^2k_-^2 - iv'k_+ & \Delta + V - \frac{2\Delta}{\gamma_1^2}v_f^2|k|^2 \end{pmatrix}. \qquad (A1)$$

This model has the corresponding eigenvalue equations

$$\begin{aligned}&\left(-\Delta + V + \frac{2\Delta}{\gamma_1^2}v_f^2|k|^2 - E\right)\varphi_B \\ &\quad + \left(\frac{1}{\gamma_1}v_F^2k_+^2 + iv'k_-\right)\varphi_A = 0, \qquad (A2)\end{aligned}$$

$$\begin{aligned}&\left(\frac{1}{\gamma_1}v_F^2k_-^2 - iv'k_+\right)\varphi_B \\ &\quad + \left(\Delta + V - \frac{2\Delta}{\gamma_1^2}v_f^2|k|^2 - E\right)\varphi_A = 0. \qquad (A3)\end{aligned}$$

We take E $\sim \Delta$ (i.e., the electron case) and solve (A2) in the nonrelativistic limit where $\|\mathrm{V}/\Delta\| \ll 1$, $\frac{2\Delta}{\gamma_1^2}v_f^2|k|^2/\Delta \ll 1$, and $|(E-\Delta)/\Delta| \ll 1$. This gives

$$\begin{aligned}\varphi_B \approx{}& \frac{1}{2\Delta}\left[1 + \frac{1}{2\Delta}\left(\frac{2\Delta}{\gamma_1^2}v_f^2|k|^2 + V - E + \Delta\right)\right] \\ &\times \left(\frac{1}{\gamma_1}v_F^2k_+^2 + iv'k_-\right)\varphi_A, \qquad (A4)\end{aligned}$$

which includes the relativistic effect up to first order. Substituting (A4) into (A3) yields

$$\begin{aligned}(E-\Delta)\varphi_A \approx{}& \left(\frac{1}{\gamma_1}v_F^2k_-^2 - iv'k_+\right)\frac{1}{2\Delta}\left[1 + \frac{1}{2\Delta}\left(\frac{2\Delta}{\gamma_1^2}v_f^2|k|^2 + V\right)\right]\left(\frac{1}{\gamma_1}v_F^2k_+^2 + iv'k_-\right)\varphi_A \\ &+ \left(\frac{1}{\gamma_1}v_F^2k_-^2 - iv'k_+\right)\frac{1}{2\Delta}\left[\frac{1}{2\Delta}(-E+\Delta)\right]\left(\frac{1}{\gamma_1}v_F^2k_+^2 + iv'k_-\right)\varphi_A - \frac{2\Delta}{\gamma_1^2}v_f^2|k|^2\varphi_A + V\varphi_A. \qquad (A5)\end{aligned}$$

In order to eliminate the energy $-E+\Delta$ on the right-hand side, we iterate the preceding expression and obtain

$$
\begin{aligned}
(E-\Delta)\varphi_A \approx & \left(\frac{1}{\gamma_1}v_F^2k_-^2 - iv'k_+\right)\frac{1}{2\Delta}\left[1+\frac{1}{2\Delta}\left(\frac{2\Delta}{\gamma_1^2}v_f^2k^2+V\right)\right]\left(\frac{1}{\gamma_1}v_F^2k_+^2+iv'k_-\right)\varphi_A \\
& -\frac{1}{8\Delta^3}\left(\frac{1}{\gamma_1}v_F^2k_-^2 - iv'k_+\right)\left(\frac{1}{\gamma_1}v_F^2k_+^2+iv'k_-\right)\left(\frac{1}{\gamma_1}v_F^2k_-^2 - iv'k_+\right)\left(\frac{1}{\gamma_1}v_F^2k_+^2+iv'k_-\right)\varphi_A \\
& -\frac{1}{4\Delta^2}\left(\frac{1}{\gamma_1}v_F^2k_-^2 - iv'k_+\right)\left(\frac{1}{\gamma_1}v_F^2k_+^2+iv'k_-\right)\left(-\frac{2\Delta}{\gamma_1^2}v_f^2k^2+V\right)\varphi_A - \frac{2\Delta}{\gamma_1^2}v_f^2k^2\varphi_A + V\varphi_A. \qquad \text{(A6)}
\end{aligned}
$$

Equation (A6) provides the Schrödinger description of conduction-band states with $E\sim\Delta$. However, we note that the corresponding Hamiltonian (denoted by $H'_{\rm eff}$) defined in (A6) is non-Hermitian and care would have to be taken if $H'_{\rm eff}$ is used in a calculation. For example, in a perturbative calculation, the perturbation theory for a non-Hermitian Hamiltonian system would have to be employed. Instead of taking the foregoing approach, we construct from $H'_{\rm eff}$ a Hamiltonian of Hermitian form for the Schrödinger model and use the Hermitian one for all calculations in this work. This construction is based on a method similar to that discussed in Appendix A of Ref. 13. Without going into mathematical details, we simply state that the Hermitian form of the Hamiltonian is given by $(H'_{\rm eff}+H'^{\dagger}_{\rm eff})/2$, which can further be organized into the form H_0+H_1 shown in Eq. (1), with H_0 being the nonrelativistic part and H_1 the first-order relativistic correction. This completes the derivation of the Schrödinger model for bilayer graphene.

We note that the Schrödinger model provides an accurate description for electron states near the gap and is valid in the vicinity of K and K' points. We estimate the range of wave vectors where the model is valid. We require the leading-order kinetic energy $\|H_0-\mathrm{V}\|\ll\Delta$. According to Eq. (1), this leads to

$$
\begin{aligned}
&-\frac{2\Delta}{\gamma_1^2}v_f^2k^2+\frac{1}{2\Delta}\left(\frac{1}{\gamma_1^2}v_F^4k^4+v\prime 2k^2\right) \\
&+\tau\frac{v\prime v_F^2}{\Delta\gamma_1}\left(3k_x^2k_y-k_y^3\right)\ll\Delta,
\end{aligned}
$$

which specifies the range.

*Corresponding author: yswu@ee.nthu.edu.tw

[1] K. S. Novoselov, A. K. Geim, S. V. Morozov, D. Jiang, Y. Zhang, S. V. Dubonos, I. V. Grigorieva, and A. A. Firsov, Science **306**, 666 (2004); K. S. Novoselov, A. K. Geim, S. V. Morozov, D. Jiang, M. I. Katsnelson, I. V. Grigorieva, S. V. Dubonos, and A. A. Firsov, Nature (London) **438**, 197 (2005); K. S. Novoselov, E. McCann, S. V. Morozov *et al.*, Nat. Phys. **2**, 177 (2006); A. K. Geim and K. S. Novoselov, Nat. Mater. **6**, 183 (2007).

[2] Y. B. Zhang *et al.*, Nature (London) **438**, 2001 (2005).

[3] M. I. Katsnelson, Nat. Phys. **2**, 620 (2006).

[4] E. McCann and V. I. Fal'ko, Phys. Rev. Lett. **96**, 086805 (2006); E. McCann, Phys. Rev. B **74**, 161403 (2006).

[5] E. V. Castro, K. S. Novoselov, S. V. Morosev, N. M. R. Peres, J. M. B. Lopes dos Santos, J. Nilsson, F. Guinea, A. K. Geim, and A. H. Castro Neto, Phys. Rev. Lett. **99**, 216802 (2007).

[6] A. H. Castro Neto, F. Guinea, N. M. R. Peres, K. S. Novoselov, and A. K. Geim, Rev. Mod. Phys. **81**, 109 (2009), and references therein.

[7] A. Rycerz, J. Tworzydlo, and C. W. J. Beenakker, Nat. Phys. **3**, 172 (2007).

[8] D. Xiao, W. Yao, and Q. Niu, Phys. Rev. Lett. **99**, 236809 (2007).

[9] I. Martin, Y. M. Blanter, and A. F. Morpurgo, Phys. Rev. Lett. **100**, 036804 (2008).

[10] J. L. Garcia-Pomar, A. Cortijo, and M. Nieto-Vesperinas, Phys. Rev. Lett. **100**, 236801 (2008).

[11] D. S. L. Abergel and T. Chakraborty, Appl. Phys. Lett. **95**, 062107 (2009).

[12] D. Gunlycke and C. T. White, Phys. Rev. Lett. **106**, 136806 (2011); D. Gunlycke *et al.*, Nano Lett. **13**, 259 (2013).

[13] G. Y. Wu *et al.*, arXiv:1104.0443; G. Y. Wu, N. Y. Lue, and L. Chang, Phys. Rev. B **84**, 195463 (2011); G. Y. Wu and N. Y. Lue, *ibid.* **86**, 045456 (2012).

[14] M.-K. Lee, N. Y. Lue, C. K. Wen, and G. Y. Wu, Phys. Rev. B **86**, 165411 (2012).

[15] Valley manipulation and valley-based devices in different materials, e.g., carbon nanotubes or silicon, have also been proposed. For a carbon-nanotube-based structure, see A. Palyi and G. Burkard, Phys. Rev. Lett. **106**, 086801 (2011); for a Si-based qubit, see D. Culcer, A. L. Saraiva, B. Koiller, X. Hu, and S. Das Sarma, *ibid.* **108**, 126804 (2012).

[16] G. Giovannetti, P. A. Khomyakov, G. Brocks, P. J. Kelly, and J. van den Brink, Phys. Rev. B **76**, 073103 (2007).

[17] B. Sachs, T. O. Wehling, M. I. Katsnelson, and A. I. Lichtenstein, Phys. Rev. B **84**, 195414 (2011).

[18] J. B. Oostinga *et al.*, Nat. Mater. **7**, 151 (2007).

[19] For QDs in bilayer graphene, see M. T. Allen *et al.*, Nat. Commun. **3**, 934 (2012).

[20] For applications based on out-of-plane pseudospins in BLG, see P. San-Jose, E. Prada, E. McCann, and H. Schomerus, Phys. Rev. Lett. **102**, 247204 (2009).

[21] P. Gosselin *et al.*, Eur. Phys. J. C **59**, 883 (2009).

[22] This state is obviously lower in energy than the alternative one-QD two-electron state with the valley triplet, for example, $|K_R(r_1)K'_R(r_2)+K_R(r_2)K'_R(r_1)\rangle\otimes|\mathcal{T}_{\rm spin}\rangle$, since the Coulomb repulsion is reduced in the valley singlet compared to that in the

valley triplet due to the electron-electron exchange interaction. This is consistent with Hund's first rule, which states that the ground state of a multielectron atom with an open subshell is the one that maximizes the total spin for all of the electrons in the subshell. In the right QD, K_R and K'_R are degenerate and form a subshell of the QD atom with two electrons to occupy it. As such, the state with the spin triplet is the ground state and it is easily accessible.

[23]M. Born and V. A. Fock, Z. Phys. A **51**, 165 (1928).

[24]We ignore the next-order correction due to $H_1^{(\text{warping})}$ and $H_1^{(\text{GVOI})}$.

[25]D. A. Lidar, I. L. Chuang, and K. B. Whaley, Phys. Rev. Lett. **81**, 2594 (1998); J. Levy, *ibid.* **89**, 147902 (2002); M. Mohseni and D. A. Lidar, *ibid.* **94**, 040507 (2005); J. M. Taylor *et al.*, Nat. Phys. **1**, 177 (2005).

[26]Long-wavelength fluctuations induce the same valley-contrasting geometric phase in the two QDs of the qubit and change the qubit state $\alpha|K_L K'_R\rangle + \beta|K'_L K_R\rangle$ only by an overall phase to $\exp(i\theta_x)(\alpha|K_L K'_R\rangle + \beta|K'_L K_R\rangle)$. Short-wavelength fluctuations may induce different geometric phase in the two QDs. In the case where the fluctuations are slowly varying in time, one can apply the method of qubit echo to remove their effect on the qubit. See Ref. 25 for details.

[27]D. P. DiVincenzo, Phys. Rev. A **51**, 1015 (1995); T. Sleator and H. Weinfurter, Phys. Rev. Lett. **74**, 4087 (1995); A. Barenco, Proc. R. Soc. London Ser. A **449**, 679 (1995).

[28]For universal spin-based quantum computing, see D. Loss and D. P. DiVincenzo, Phys. Rev. A **57**, 120 (1998); G. Burkard, D. Loss, and D. P. DiVincenzo, Phys. Rev. B **59**, 2070 (1999).

[29]M. A. Nielsen and I. L. Chuang, *Quantum Computation and Quantum Information* (Cambridge University Press, Cambridge, 2003), and references therein.

[30]The AGNR states in BLG are similar to those in monolayer graphene. For the latter, see L. Brey and H. A. Fertig, Phys. Rev. B **73**, 235411 (2006).

[31]S. Datta and B. Das, Appl. Phys. Lett. **56**, 665 (1990).

[32]The warping terms alone do not contribute to subband splitting. This can be shown by noting that even in the presence of a gate field, the transformation $\psi(x,y) \to \psi(-x,y)^*$ for a subband wave function $\psi(x,y)$ [$\psi(x,y) = \exp(ik_x x)\varphi(y)$] transforms a K-valley state to a K'-valley state and vice versa, in the absence of $H_1^{(\text{GVOI})}$. In other words, it shows that for any given k_x, a K-valley state is always degenerate with a K'-valley state if $H_1^{(\text{GVOI})}$ is ignored. Therefore, in this case, there is no subband splitting due to the warping terms alone. However, analysis shows that there may be higher-order contributions if both $H_1^{(\text{GVOI})}$ and the warping terms are included. For the evaluation of leading-order contributions, we omit $H_0^{(\text{warping})}$ and $H_1^{(\text{warping})}$ here.

[33]A. Wirthmann *et al.*, Physica E **34**, 493 (2006).

[34]A. F. Morpurgo and F. Guinea, Phys. Rev. Lett. **97**, 196804 (2006).